Biogeosciences, 13, 691–705, 2016
www.biogeosciences.net/13/691/2016/
doi:10.5194/bg-13-691-2016

Biogeosciences Open Access EGU

Fate of terrestrial organic carbon and associated CO_2 and CO emissions from two Southeast Asian estuaries

D. Müller[1,2], T. Warneke[1], T. Rixen[2,3], M. Müller[4], A. Mujahid[5], H. W. Bange[6], and J. Notholt[1,7]

[1]Institute of Environmental Physics, University of Bremen, Otto-Hahn-Allee 1, 28359 Bremen, Germany
[2]Leibniz Center for Tropical Marine Ecology, Fahrenheitstr. 6, 28359 Bremen, Germany
[3]Institute of Geology, University of Hamburg, Bundesstr. 55, 20146 Hamburg, Germany
[4]Swinburne University of Technology, Faculty of Engineering, Computing and Science, Jalan Simpang Tiga, 93350 Kuching, Sarawak, Malaysia
[5]Department of Aquatic Science, Faculty of Resource Science and Technology, University Malaysia Sarawak, 94300 Kota Samarahan, Sarawak, Malaysia
[6]GEOMAR Helmholtz Centre for Ocean Research Kiel, Düsternbrooker Weg 20, 24105 Kiel, Germany
[7]MARUM Center for Marine Environmental Sciences, University of Bremen, Leobener Str., 28359 Bremen, Germany

Correspondence to: D. Müller (dmueller@iup.physik.uni-bremen.de)

Received: 4 May 2015 – Published in Biogeosciences Discuss.: 5 June 2015
Revised: 6 January 2016 – Accepted: 14 January 2016 – Published: 4 February 2016

Abstract. Southeast Asian rivers convey large amounts of organic carbon, but little is known about the fate of this terrestrial material in estuaries. Although Southeast Asia is, by area, considered a hotspot of estuarine carbon dioxide (CO_2) emissions, studies in this region are very scarce. We measured dissolved and particulate organic carbon, as well as CO_2 partial pressures and carbon monoxide (CO) concentrations in two tropical estuaries in Sarawak, Malaysia, whose coastal area is covered by carbon-rich peatlands. We surveyed the estuaries of the rivers Lupar and Saribas during the wet and dry season, respectively. Carbon-to-nitrogen ratios suggest that dissolved organic matter (DOM) is largely of terrestrial origin. We found evidence that a large fraction of this carbon is respired. The median pCO_2 in the estuaries ranged between 640 and 5065 µatm with little seasonal variation. CO_2 fluxes were determined with a floating chamber and estimated to amount to 14–268 mol m^{-2} yr^{-1}, which is high compared to other studies from tropical and subtropical sites. Estimates derived from a merely wind-driven turbulent diffusivity model were considerably lower, indicating that these models might be inappropriate in estuaries, where tidal currents and river discharge make an important contribution to the turbulence driving water–air gas exchange. Although an observed diurnal variability of CO concentrations suggested that CO was photochemically produced, the overall concentrations and fluxes were relatively moderate (0.4–1.3 nmol L^{-1} and 0.7–1.8 mmol m^{-2} yr^{-1}) if compared to published data for oceanic or upwelling systems. We attributed this to the large amounts of suspended matter (4–5004 mg L^{-1}), limiting the light penetration depth and thereby inhibiting CO photoproduction. We concluded that estuaries in this region function as an efficient filter for terrestrial organic carbon and release large amounts of CO_2 to the atmosphere. The Lupar and Saribas rivers deliver 0.3 ± 0.2 Tg C yr^{-1} to the South China Sea as organic carbon and their mid-estuaries release approximately 0.4 ± 0.2 Tg C yr^{-1} into the atmosphere as CO_2.

1 Introduction

Estuaries are net heterotrophic systems (Duarte and Prairie, 2005; Cole et al., 2007) and act as a source of carbon dioxide (CO_2) to the atmosphere, releasing 150 Tg C annually (Laruelle et al., 2013). Southeast Asia is considered one of the hotspot regions of aquatic CO_2 emissions to the atmosphere (Regnier et al., 2013), because many Southeast Asian rivers exhibit high organic carbon concentrations (Alkhatib et al., 2007; Moore et al., 2011, 2013; Müller et al., 2015). It has been estimated that Indonesian rivers alone account for

10 % of the dissolved organic carbon (DOC) exported to the ocean globally (Baum et al., 2007), which was attributed to the presence of tropical peatlands. Southeast Asian peatlands store 68.5 Gt carbon (Page et al., 2011) and represent a globally important carbon pool. DOC concentrations in Southeast Asian peat-draining rivers range up to 5667 µmol L^{-1} (Moore et al., 2013). Although a small fraction of this DOC is respired in the river and released to the atmosphere as CO_2, the larger part is transported downstream (Müller et al., 2015), ultimately reaching the estuary and the coastal ocean. So far, the fate of this carbon fraction remains unclear, and data particularly in this region are scarce.

Peat-derived organic matter consists mainly of lignin and its derivates (Andriesse, 1988) and is thus relatively recalcitrant to degradation. In addition, short water residence times constrain organic matter decomposition (Müller et al., 2015). However, high organic carbon loads and high temperatures suggest high microbial activity both in the water column and in the sediments, leading to high decomposition rates.

Additionally, photodegradation was proposed as an important removal mechanism for terrestrial organic matter in the ocean (Miller and Zepp, 1995). Chromophoric dissolved organic matter (CDOM) absorbs light, mainly in the UV region. The absorbed photons initiate abiotic photochemical reactions, during which carbon monoxide (CO) and CO_2 are produced (Stubbins, 2001), with the CO_2 production being 14 to 20 times larger than CO production (Vähätalo, 2010). Photochemistry might be of particular importance in estuaries (Ohta et al., 2000), where dissolved organic matter (DOM) is largely of terrestrial origin. Terrestrial CDOM was found to be more efficient in producing CO than marine CDOM (Zhang et al., 2006), making estuaries a significant source of CO to the atmosphere (Valentine and Zepp, 1993). Ultimately, recalcitrant terrestrial organic matter might be subject to photobleaching (Vähätalo, 2010), increasing its bioavailability to the heterotrophic community.

In order to investigate whether and how terrestrial organic carbon is processed in tropical estuaries, we studied organic carbon, dissolved CO_2 and CO in two Malaysian estuaries, both of which receive terrestrial carbon from rivers draining a catchment that is partially covered by peat.

2 Materials and methods

2.1 Study area

Sarawak is Malaysia's largest state and is located in the northwest of the island of Borneo, which is divided between Indonesia, Brunei and Malaysia. It is separated from peninsular Malaysia by the South China Sea. Sarawak has a tropical climate. The mean annual air temperature in Sarawak's capital Kuching (1.56° N, 110.35° E) is 26.1 °C (average 1961–1990, DWD, 2007). Rainfall is high throughout the year, but pronounced during the northeastern monsoon, which occurs between November and February.

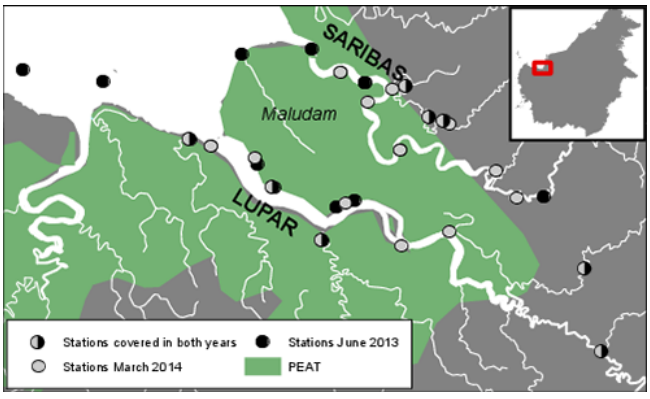

Figure 1. Map of the study area. The stations are indicated by the grey and black dots; peat soils (histosols) are indicated in green (as of FAO, 2009).

Our study focused on two macrotidal estuaries in western Sarawak (tidal range 3–4 m). The coastal area of western Sarawak is covered by peatlands. The largest peat dome is found on the Maludam peninsula. It is rainwater-fed and covered by dense peat swamp forest, which has been protected ever since Maludam was gazetted as a national park in 2000. The peninsula is enclosed by the rivers Lupar and Saribas (Fig. 1), which originate in upland areas. Six channels from the Maludam peat swamp forest drain into the Lupar estuary and six into the Saribas, respectively (Kselik and Liong, 2004). With reference to their catchment areas, the peat coverage in the Lupar and Saribas basins is 30.5 and 35.5 %, respectively (FAO, 2009), whereas the peat is located very close to the coast (Fig. 1). The catchment sizes are 6558 km^2 (Lupar) and 1943 km^2 (Saribas) (Lehner et al., 2006).

Sampling was performed during two ship cruises in 2013 and 2014. The 2013 cruise took place in June (18–23 June) during the dry season. The 2014 cruise was performed in March (10–19 March), right after the end of the monsoon season. We sampled 20 stations in 2013 and 23 stations in 2014 (Fig. 1). Here, we report the data separately for the lower (salinity > 25), middle (salinities 2–25) and upper (salinity < 2) estuaries. In 2014, we went further upstream than in 2013. Therefore, when it comes to the mid-estuaries, we report medians for the "2013 spatial extent", i.e., refer to the spatial coverage of 2013.

2.2 Discharge and flow velocity

We estimated river discharge (Q) from the difference between precipitation (P) and evapotranspiration (ET). Precipitation was taken from NOAA NCEP Reanalysis data set for the nearest upstream grid (0.95° N, 110.625° E, www.esrl.noaa.gov/psd/data/reanalysis/reanalysis.shtml). Evapotranspiration was taken from the literature (Kumagai et al.,

2005). Ultimately, we derived $Q = (P - \mathrm{ET}) \cdot A$, where A is the catchment area (m^2). The rivers' flow velocity was estimated from the drift during the stations, when the boat drifted freely. To this end, we used the GPS information of a CTD at the beginning and the end of the cast, and the duration of the cast to calculate the flow velocity (2014 data only). Note that as boat drift might have been affected by wind, these flow velocity estimates have limited accuracy. However, a very rough estimate of flow velocity is sufficient for our purposes.

2.3 Water chemistry

Salinity and temperature profiles were measured at each station with a CastAway CTD (conductivity, temperature, depth; Sontek, USA). Additionally, water pH, dissolved oxygen (DO), and conductivity were measured in the surface water with a Multi3420, using an FDO 925 oxygen sensor, a SenTix 940 pH sensor, and a TetraCon 925 conductivity sensor (WTW, Germany). The pH sensor was calibrated with NIST (National Institute of Standards and Technology, formerly National Bureau of Standards, NBS) traceable buffers and is reported on NBS scale. Apparent oxygen utilization (AOU) was calculated as the difference between the saturation oxygen concentration and the measured oxygen concentration.

$$\mathrm{AOU} = O_2^{\mathrm{sat}} - O_2^{\mathrm{meas}} \quad (1)$$

Oxygen solubility for a given temperature and salinity was calculated with constants from Weiss (1970).

Samples for determination of dissolved inorganic nitrogen (DIN) concentrations were taken at every station from approximately 1 m below the water surface. The water was filtered through a Whatman glass microfiber filter (pore size 0.7 µm), preserved with a mercuric chloride ($HgCl_2$) solution and stored cooled and upright until analysis (approx. 2 months after sampling). Concentrations of nitrate (NO_3^-), nitrite (NO_2^-) and ammonia (NH_4^+) were determined spectrophotometrically (Grasshoff et al., 1999) with a Continuous Flow Analyzer (Alliance, Austria).

2.4 Organic carbon and carbon isotope analysis

Dissolved organic carbon (DOC) samples were filtered (pore size 0.45 µm) and acidified with 21 % phosphoric acid (H_3PO_4) until the pH had dropped below 2. Samples were stored frozen until analysis (approx. 2 months after sampling). DOC concentrations were determined through high temperature combustion and subsequent measurement of the evolving CO_2 with a non-dispersive infrared detector. In 2014, those samples were also analyzed for total dissolved nitrogen (TDN) using a TOC-VCSH with a TNM-1 analyzer (Shimadzu, Japan). Dissolved organic nitrogen (DON) was then calculated by subtracting DIN from TDN.

Particulate material was sampled by filtering water through pre-weighed and pre-combusted Whatman glass fiber filters. The net sample weight was determined. 1 N hydrochloric acid was added in order to remove inorganic carbon and samples were dried at 40 °C. Organic carbon and nitrogen contents were determined by flash combustion with a Euro EA3000 Elemental Analyzer (Eurovector, Italy). The abundance of the stable isotope ^{13}C was determined with a Finnigan Delta plus mass spectrometer (Thermo Fisher Scientific, USA).

Samples for determination of $\delta^{13}C$ in dissolved inorganic carbon (DIC) were preserved with $HgCl_2$, sealed against ambient air and stored cool, upright and in the dark until analysis (3–4 months after sampling). 10 mL vials were prepared with 50 µL of 98 % H_3PO_4 and a He headspace. Depending on the salinity, 1–4 mL sample volume was injected through the septum using a syringe. The prepared sample was allowed to equilibrate for 18 h and the ^{13}C / ^{12}C ratio was determined with mass spectrometry (MAT 253, Thermo Scientific, USA). $\delta^{13}C$ values are reported against Pee Dee Belemnite (PDB).

2.5 CO_2 and CO measurements

In order to determine partial pressures of dissolved CO_2 and CO in the water, we used a Weiss equilibrator (Johnson, 1999). Water from approximately 1 m below the surface was pumped through the equilibrator at a rate of approximately 20 L min^{-1}. Dry air mole fractions of CO_2 and CO in the equilibrator's headspace were determined with an in situ Fourier Transform InfraRed (FTIR) trace gas analyzer. The instrument was manufactured at the University of Wollongong, Australia, and is described in detail by Griffith et al. (2012). The equilibrator headspace air circulated between the FTIR and the equilibrator at a rate of 1 L min^{-1} in a closed loop, whereas the air was dried before entering the analyzer using a Nafion® drier and a magnesium perchlorate moisture trap (Griffith et al., 2012). The equilibrator and the sampling lines were covered with aluminum foil to avoid CO photoproduction in the sampled air. FTIR spectra were averaged over 5 min, and dry air mole fractions were retrieved using the MALT5 software (Griffith, 1996). The gas dry air mole fractions were corrected for pressure, water and temperature cross-sensitivities with empirically determined factors (Hammer et al., 2013). Calibration was performed twice during each ship cruise with a suite of gravimetrically prepared gas mixtures (Deuste Steininger) ranging from 380 to 10 000 ppm CO_2 and 51 to 6948 ppb CO. Those gas mixtures were calibrated against the World Meteorological Organization (WMO) reference scale at the Max Planck Institute for Biogeochemistry in Jena, Germany.

Water temperature was measured both in the equilibrator and in the water using a Pico PT-104 temperature data recorder (Pico Technology, UK). Ambient air temperature and pressure were recorded over the entire cruise with an SP-1016 temperature data recorder and a PTB110 barometer (Vaisala, Finland), respectively. Gas partial pressures for

dry air ($p\mathrm{Gas}_{\mathrm{dryair}}$) were calculated from the FTIR measurements and our records of ambient pressure. We corrected for the removal of water (Dickson et al., 2007) using

$$p\mathrm{Gas} = p\mathrm{Gas}_{\mathrm{dryair}}(1 - \mathrm{VP}(H_2O)), \quad (2)$$

where pGas is the corrected gas partial pressure and VP(H_2O) is the water vapor pressure, which was calculated with the equation given in Weiss and Price (1980).

Equilibrator measurements have been widely used for trace gas measurements in estuarine surface water (Chen et al. (2013) and references therein). For CO_2, the response time is usually short (< 10 min) and the error associated with a remaining disequilibrium between water and headspace air is 0.2 % for a Weiss equilibrator (Johnson, 1999). CO, in contrast, takes much longer to reach full equilibrium, and an error of up to 25 % must be taken into account for measurements with a Weiss equilibrator (Johnson, 1999).

In the freshwater region, we were unable to carry out FTIR measurements, because the sampling spots could not be reached by ship. Instead, we performed headspace equilibration measurements of discrete samples with an Li-820 CO_2 analyzer (LICOR, USA), which was calibrated with the same secondary standards as the FTIR. We filled a 10 L canister with 9.5 L of sample water (2014: 0.6 L flask filled with 0.35 L of sample water) and left ambient air in the headspace. We connected the Li-820 analyzer inlet to the headspace and the outlet to the bottom of the canister, so that air could bubble through the sample water, accelerating the equilibration process. The $p\mathrm{CO}_2$ obtained from headspace equilibration measurements was corrected for water vapor pressure as well.

Following common practice, we will report CO_2 levels in terms of CO_2 partial pressure ($p\mathrm{CO}_2$), but convert CO partial pressure to molar concentrations using solubilities according to Wiesenburg and Guinasso (1979).

2.6 Flux estimation

In 2014, we performed direct flux measurements with a floating chamber. The floating chamber was an upside-down flower pot with a volume of 8.7 L and a surface area of 0.05 m^2 which it enclosed with the water. Its walls extended 1 cm into the water. The chamber headspace was connected to the Li-820 CO_2 analyzer, and CO_2 concentrations in the chamber were recorded over time. The concentration change was fitted linearly and the water-to-air CO_2 flux F (in $\mu\mathrm{mol}\,\mathrm{m}^{-2}\,\mathrm{s}^{-1}$) was calculated according to

$$F = \frac{\mathrm{d}c}{\mathrm{d}t}\frac{pV}{\mathrm{RTA}}, \quad (3)$$

where $\frac{\mathrm{d}c}{\mathrm{d}t}$ is the slope of the fitted curve ($\mu\mathrm{mol}\,\mathrm{mol}^{-1}\,\mathrm{s}^{-1}$), p is the pressure (Pa), V is the chamber volume (m^3), R is the universal gas constant, T the temperature (K) and A the surface area (m^2). The gas exchange velocity was calculated with

$$k_{\mathrm{CO}_2} = \frac{F}{K_0\left(p\mathrm{CO}_2^{\mathrm{water}} - p\mathrm{CO}_2^{\mathrm{air}}\right)}, \quad (4)$$

where k_{CO_2} is the gas exchange velocity ($\mathrm{m}\,\mathrm{s}^{-1}$) of CO_2 and $p\mathrm{CO}_2^{\mathrm{air}}$ is the atmospheric CO_2 partial pressure, which was measured with the Li-820 CO_2 analyzer during the cruises. For comparisons, k_{CO_2} was normalized to a Schmidt number of 600 (Schmidt number Sc relates the diffusivity of the gas to the viscosity of the water):

$$\frac{k_{600}}{k_{\mathrm{CO}_2}} = \left(\frac{600}{\mathrm{Sc}_{\mathrm{CO}_2}}\right)^{-n}, \quad (5)$$

with $n = 0.5$ for rough surfaces (Jähne et al., 1987). Schmidt numbers were calculated from water temperature for both saline and freshwater (Wanninkhof, 1992), and evaluated for the in situ salinity assuming a linear dependency (Borges et al., 2004). CO_2 fluxes were calculated for every data point using updated solubilities, $p\mathrm{CO}_2$ values and exchange velocities and the average atmospheric partial pressure. The two estimates that were obtained for the two different seasons (2013 spatial extent) were averaged and the uncertainty was estimated from the uncertainty associated with the gas exchange velocity, which proved to cause the largest error.

The relationship with the Schmidt number was also exploited for calculating CO fluxes. Schmidt numbers for CO were calculated using the coefficients given in Raymond et al. (2012) for freshwater, and the formula given in Zafiriou et al. (2008) for saltwater. Atmospheric CO mole fractions were obtained from the NOAA ESRL Carbon Cycle Cooperative Global Air Sampling for the nearest station (Novelli and Masarie, 2014), which was Bukit Kototabang, Indonesia (0.202° S, 100.3° E). Atmospheric CO monthly averages from the NOAA ESRL data set were available from 2004 to 2013. For our dry season data, we used the monthly average for June 2013, and for our wet season data, we calculated the average CO mixing ratio in March for the years that were available. CO fluxes were then calculated in the same way as CO_2 fluxes.

Since many flux estimates in the literature were obtained using exchange velocities derived from empirical equations, we calculated k also using the wind speed parameterization from Wanninkhof (1992) for comparison. Wind speed data were taken from the NOAA NCEP Reanalysis data set for the closest coastal grid (2.85° N, 110.625° W). Here, we chose the most downstream grid because the upstream grid, which we picked for precipitation, is over land, where wind speeds might be much lower than in the estuary. We considered daily wind speeds for the time period of both our 2013 and 2014 cruise.

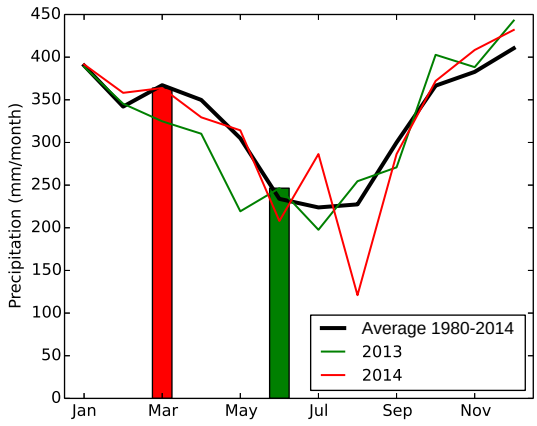

Figure 2. Average monthly precipitation during 1980–2014 (black), and monthly precipitation in 2013 (green) and 2014 (red). The bars indicate the rainfall during our sampling months. It can be seen that the rainfall pattern was not much different from the historical average during these periods.

3 Results

3.1 Discharge

Annual average precipitation from 1980 to 2014 amounted to 3903 mm yr^{-1} in the chosen grid, corresponding to an average precipitation of 325 mm $month^{-1}$. The precipitation during June 2013 was below average (246 mm) and above average (364 mm) in March 2014. Both values do not deviate much from the historical averages during 1980–2014 (March: 367 mm; June: 234 mm; see Fig. 2). In the following, we will refer to our measurements in June 2013 as representative of the dry season, and those in March 2014 as representative of the wet season.

With an average evapotranspiration of 4.2 mm d^{-1} (Kumagai et al., 2005), we estimated the average annual discharge for the Lupar river to be 490 and 160 $m^3 s^{-1}$ for the Saribas river. The flow velocities were estimated to be 2.5 ± 1.4 m s^{-1} (average ± largest deviation from average) for the Lupar river, 0.7 ± 0.7 m s^{-1} for the Saribas, and 0.8 ± 1.0 m s^{-1} for the Saribas tributary. Note that the measurements were taken during different stages of the tidal cycle, which explains the large variability.

3.2 Water chemistry

Our data covered a salinity range of 0–30.6 in the dry season and 0–31.0 in the wet season. Although relatively higher surface salinities were observed further upstream during the dry season if compared to the wet season, the geographical location of the mid-estuaries largely overlapped (Fig. 5a, b). pH ranged between 6.7 and 8.0 in the dry season (2013) and between 6.8 and 7.6 in the wet season (2014) and was positively correlated with surface salinity ($r = 0.8$, data from both years). Notably, at salinity zero, pH was higher than suggested by this correlation, and ranged between 6.7 and 7.3 (both seasons).

DIN concentrations in the surface water were generally rather low. During the dry season, DIN ranged between 1.7 and 87.1 µmol L^{-1}, whereas most concentrations were between 15 and 30 µmol L^{-1}. In the wet season, DIN concentrations ranged between 3.4 and 21.7 µmol L^{-1}. The medians for the individual estuaries show that overall, DIN concentrations were slightly higher in the dry season (Table 1).

Dissolved oxygen was mostly slightly undersaturated. Oxygen saturation in the surface water was lower in the dry season than in the wet season (Table 1), with oxygen saturation ranging between 63.6–94.6 % (2013) and 79.0–100.4 % (2014). These values correspond to an AOU between 14 and 93 µmol L^{-1} (2013) and −1 and 52 µmol L^{-1} (2014), respectively. Negative AOU suggests net oxygen production and was only observed once in the lower estuary.

3.3 Organic carbon

DOC ranged from 80 to 784 µmol L^{-1} in the dry season and from 172 to 1180 µmol L^{-1} in the wet season and was negatively correlated with salinity (Fig. 3), indicating that freshwater supplies DOC to the estuary, while seawater has a dilution effect. However, the end-member determined from the salinity-DOC correlation was not confirmed by the samples taken in the upper estuaries: the calculated end-member for Lupar was 673 ± 274 µmol L^{-1} (intercept of the regression curve ± standard error of the estimate), and the measured freshwater DOC median was 89 µmol L^{-1} (2013) and 208 µmol L^{-1} (2014). For Saribas, the calculated end-member was 425 ± 54 µmol L^{-1}, and the measured value was 312 µmol L^{-1} (2013, Table 1). This discrepancy indicates that there is a source of DOC in the estuaries. With regards to their location, peatlands seemed a likely source of carbon to the estuaries. In a different study, we found DOC concentrations in a peat-draining river on the Maludam peninsula between 3612 and 3768 µmol L^{-1} (Müller et al., 2015). With the average (3690 µmol L^{-1}) as a second zero-salinity end-member, we estimated how much carbon derives from peat-draining tributaries from the Maludam peninsula using a simple three-point mixing model (Fig. 3). The Maludam contribution f (in %) was calculated as

$$f = \frac{\mathrm{EM_{calc}} - \mathrm{EM_{meas}}}{\mathrm{EM_{Maludam}} - \mathrm{EM_{meas}}} \cdot 100, \quad (6)$$

with $\mathrm{EM_{calc}}$ the calculated end-member, $\mathrm{EM_{meas}}$ the measured end-member and $\mathrm{EM_{Maludam}}$ the peat-draining rivers' end-member. Accordingly, 15 % of the DOC in the Lupar river is derived from these peat-draining tributaries, and 3 % of DOC in the Saribas river. Following Baum et al. (2007), the total DOC export to the ocean from Lupar and Saribas was estimated from the calculated zero-salinity end-members (673 and 425 µmol L^{-1}, respectively), assuming that they provide an average of non-peat and peat freshwa-

Table 1. Dissolved organic carbon (DOC), particulate organic carbon (POC) and dissolved inorganic nitrogen (DIN) median concentrations and oxygen saturation in the Lupar and Saribas estuaries.

	DOC (µmol L^{-1})		POC (µmol L^{-1})		DIN (µmol L^{-1})		DO (%)	
	Dry	Wet	Dry	Wet	Dry	Wet	Dry	Wet
Lupar LE	142*	n.d.	62*	n.d.	7*	n.d.	n.d.	n.d.
Saribas LE	n.d.	244*	n.d.	42*	n.d.	18*	n.d.	100.4*
Lupar ME	340	338	456	650	22	20	70.8	94.4
Saribas ME	258	281	766	292	30	14	82.8	85.8
Saribas tributary	685	374	2040	281	22	11	n.d.	82.8
Lupar UE	89	208	79	131	5	5	84.4	93.3
Saribas UE	312*	n.d.	4114*	n.d.	19*	n.d.	63.6*	n.d.

LE: lower estuary (salinity > 25). ME: mid-estuary (salinity 2–25, for the 2013 spatial extent of the rivers). UE: upper estuary.
* denotes that only one data point was available.

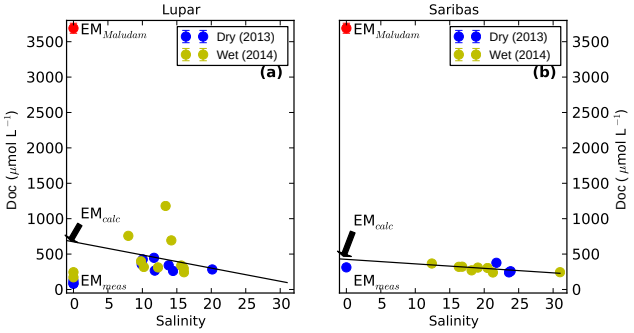

Figure 3. Dissolved organic carbon (DOC) concentrations vs. salinity in the Lupar **(a)** and Saribas **(b)** estuaries. The red marker refers to the zero salinity end-member in the peat-draining tributaries. The line indicates the DOC-salinity regression line; labels refer to theoretical and measured end-member values as described in the text.

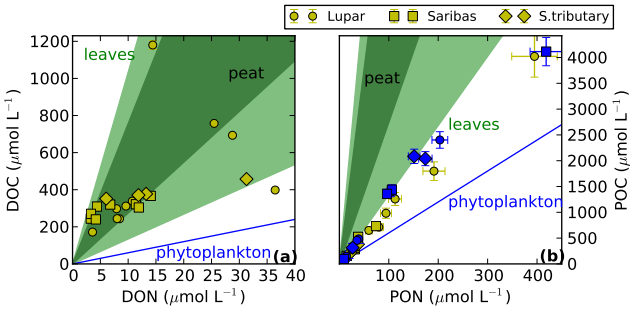

Figure 4. Carbon-to-nitrogen (C/N) ratios in dissolved organic matter **(a)** and in particulate organic matter **(b)**. Blue markers refer to samples from 2013; yellow markers refer to samples from 2014. The individual rivers are denoted by different symbols. Lines refer to the C/N ratios that would be expected for tropical peat and leaves (Baum, 2008) and for phytoplankton. Note that DON data shown in panel **(a)** were only available in 2014.

ter inputs, and annual average discharge. Accordingly, Lupar and Saribas together convey 0.15 ± 0.05 Tg yr^{-1} DOC to the South China Sea (Table 4).

Both the Lupar and Saribas estuaries were very turbid. Suspended particulate matter (SPM) ranged from 3.7 to 5003.6 mg L^{-1} in 2013 and from 13.8 to 3566.7 mg L^{-1} in 2014. Particulate organic carbon (POC) was higher during the dry season (Table 1), ranging from 51 to 4114 µmol L^{-1} in 2013 and from 17 to 2907 µmol L^{-1} in 2014. The atomic carbon-to-nitrogen (C/N) ratio of particulate organic matter (POM) ranged between 8.5 and 14.1 in 2013 and between 8.1 and 13.8 in 2014 (see Fig. 4b). δ^{13}C values ranged between −28.5 and −25.5 ‰ in 2013 and between −27.6 and −24.4 ‰ in 2014. In contrast, the C/N ratio in the dissolved organic matter (DOM) was much higher: it ranged between 10.9 and 81.8 (2014 data; see Fig. 4a), whereas the lowest value was measured on the Lupar river, upstream of the Maludam peninsula, and the highest value was measured on the Lupar river at the mouth of a peat-draining left-bank tributary (see Fig. 1). The average for all samples was 40.6.

Since POC was not conservatively transported through the estuary, the export of POC to the South China Sea was estimated from the median POC concentration and discharge (see the Supplement). 0.10 Tg C yr^{-1} are estimated to be delivered from the Lupar, and another 0.03 Tg C yr^{-1} from the Saribas (Table 4). Taken together with the DOC export, this implies that Lupar and Saribas deliver approximately 0.3 ± 0.2 Tg organic carbon to the South China Sea every year, approximately half of which is bound to particles.

3.4 CO_2 and CO

In both years, both CO_2 and CO were found to be above atmospheric equilibrium, indicating that the Lupar and Saribas estuaries were net sources of these gases to the atmosphere.

pCO_2 ranged from 297 to 5504 µatm in 2013 and from 327 to 5014 µatm in 2014. pCO_2 increased with decreasing salinity, indicating that high pCO_2 can be attributed to freshwater input (Fig. 5). However, matters were different for the freshwater samples. The measured freshwater end-member pCO_2

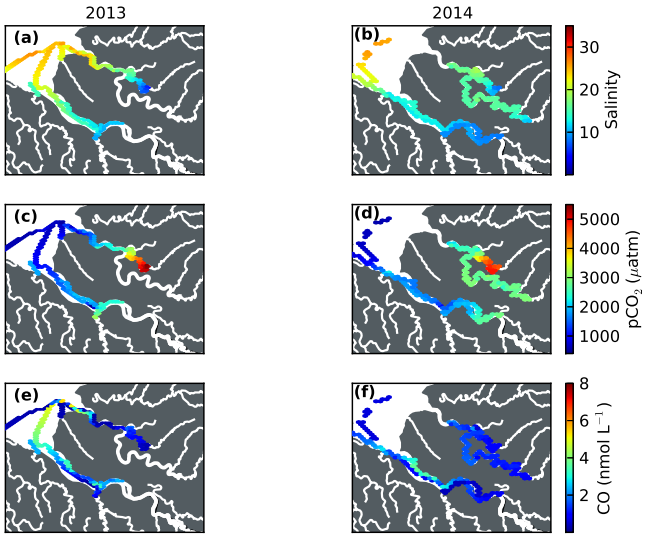

Figure 5. Salinity (**a**, **b**), CO_2 partial pressures (**c**, **d**) and CO concentrations (**e**, **f**) measured during the two cruises in 2013 (left column) and 2014 (right column).

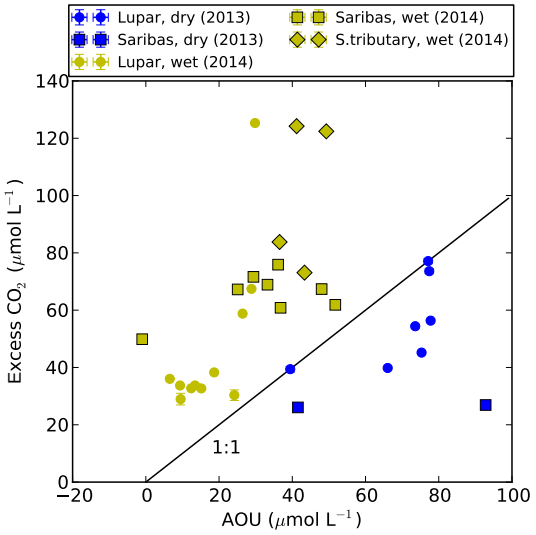

Figure 6. Apparent oxygen utilization (AOU) vs. excess CO_2. Blue markers refer to samples from 2013; yellow markers refer to samples from 2014. The individual rivers are denoted by different symbols.

was relatively moderate (1021–1527 µatm). Table 2 summarizes the median pCO_2 values in the lower, mid- and upper estuaries. It can be seen that like DOC, pCO_2 was highest in the mid-estuaries. The difference between dry and wet season pCO_2 was marginal (see Fig. 5). Excess CO_2 (in µmol L^{-1}) was correlated with AOU for the Lupar river (dry season: $r = 0.71$, $p = 0.01$; wet season: $r = 0.62$, $p = 0.14$). For the Saribas, the correlation was weak in the dry season ($r = 0.52$, $p = 0.18$). Due to the limited number of data points, no correlation could be established for the Saribas during the wet season (see Fig. 6).

Interestingly, Saribas and its tributary had a higher pCO_2 (i.e., higher pCO_2 at the same salinity) than Lupar, but not higher DOC. δ^{13}C-DIC ranged from −0.85 ‰ in the lower estuary to −15.70 ‰ in the freshwater region and increased with increasing salinity (not shown).

CO ranged from < 0.1 to 5.8 nmol L^{-1} (< 0.1 to 7.2 µatm) in the dry season (2013) and from 0.2 to 12.4 nmol L^{-1} (0.3 to 14.7 µatm) in the wet season (2014) and was spatially variable (Fig. 5). Median values are summarized in Table 2. CO concentrations were higher during daytime than during the night, independent of the boat's location (Fig. 7). In both years, maximum CO concentrations were observed around noon and in the early afternoon. CO concentrations were not correlated with salinity, DOC, POC or SPM (not shown).

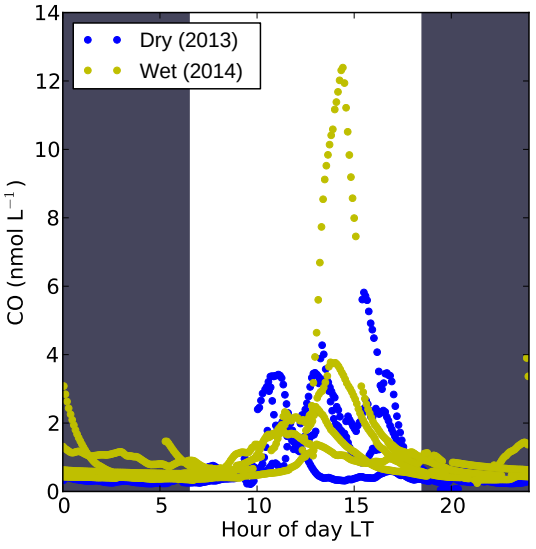

Figure 7. CO concentrations depending on the hour of the day local time. The black areas refer to nighttime hours, while the light area denotes the daylight hours. All data are gathered in this figure; 2013 and 2014 data are distinguished with different colors and symbols. Note that the boat was usually moving during daytime and more often not moving during nighttime.

3.5 CO_2 and CO fluxes

The CO_2 fluxes measured with the floating chamber showed large spatial variations and ranged from 63 to 935 mmol m^{-2} d^{-1}. The lowest flux was measured in the Saribas mid-estuary, and the highest flux was measured on the Saribas tributary. $k_{600,FC}$ values were averaged for the individual rivers and are reported with the largest deviation of a single measurement from the mean. The Saribas tributary, which was the smallest of the studied rivers, had the highest $k_{600,FC}$ of 23.9 ± 14.8 cm h^{-1}. The largest river, Lupar, had a high $k_{600,FC}$ of 20.5 ± 4.9 cm h^{-1} as well, which is probably due to the high flow velocity (2.5 m s^{-1}). The Saribas main river had a $k_{600,FC}$ of 13.2 ± 11.0 cm h^{-1}, with

Table 2. Median CO_2 partial pressures and CO concentrations (and partial pressures in brackets), respectively.

	pCO_2 (µatm)		CO (nmol L^{-1}) (µatm)	
	Dry	Wet	Dry	Wet
Lupar LE	640 ± 105	662 ± 36	0.4 ± 2.5 [0.45 ± 3.08]	0.7 ± 0.1 [0.82 ± 0.02]
Saribas LE	n.d.	n.d.	n.d.	n.d.
Lupar ME	2462 ± 574	1849 ± 881	1.3 ± 1.1 [1.48 ± 1.29]	0.5 ± 2.7 [0.57 ± 3.24]
Saribas ME	2250 ± 416	2235 ± 304	0.4 ± 0.7 [0.50 ± 0.83]	0.7 ± 0.7 [0.79 ± 0.83]
Saribas tributary	5065 ± 840	2925 ± 789	0.5 ± 0.7 [0.55 ± 0.78]	0.4 ± 0.5 [0.52 ± 0.57]
Lupar UE	1527 ± 38	1021 ± 357	n.d.	n.d.
Saribas UE	1159 ± 29	n.d.	n.d.	n.d.

LE: lower estuary (salinity > 25). ME: mid-estuary (salinity 2–25, for the 2013 spatial extent of the rivers). UE: upper estuary. Values are median ± 1 standard deviation.

large spatial variability. The wind speed averaged 3.0 m s^{-1} during our 2013 sampling period and 2.3 m s^{-1} during the 2014 sampling period. The average $k_{600,W92}$ calculated with W92 were 1 order of magnitude lower than the experimentally determined ones, with 3.1 cm h^{-1} during the dry season and 1.9 cm h^{-1} during the wet season.

Atmospheric pCO_2 averaged 403.6 µatm in the dry season (2013) and 414.4 µatm in the wet season (2014). Atmospheric CO was 77.91 ppb in June 2013, corresponding to 77.49 natm. The average monthly mean for March was 145.93 ppb, corresponding to 145.58 natm. The calculated CO_2 and CO fluxes in the lower, mid- and upper estuaries are summarized in Table 3. Fluxes for the lower estuary were derived for the Lupar river (Fig. 5). Estimates for the upper estuaries were based on our pCO_2 measurements in the freshwater region and the average $k_{600,FC}$ of Lupar and Saribas, respectively (Table 3). CO_2 fluxes determined with the floating chamber ($F_{CO_2,FC}$) ranged between 14 and 268 mol m^{-2} yr^{-1} and CO fluxes ($F_{CO,FC}$) between 0.7 and 1.8 mmol m^{-2} yr^{-1}. For comparison, using $k_{600,W92}$, we obtained CO_2 fluxes between 2 and 30 mol m^{-2} yr^{-1}.

Like pCO_2, the CO_2 fluxes were highest in the mid-estuaries, with $F_{CO_2,FC}$ ranging between 73 and 268 mol m^{-2} yr^{-1}. The CO flux from Lupar was twice as high in the mid-estuary than in the lower estuary.

In order to calculate the total flux from these estuaries, we estimated the estuarine surface area of both systems in ArcGIS (for details see the Supplement). The Lupar estuary has a surface area of 220 km^2, which corresponds to 3 % of the catchment area, and the Saribas (excluding the tributary) estuary has a surface area of 102 km^2 (5 % of the catchment). The total water–atmosphere flux for the Lupar was 0.30 ± 0.09 and 0.09 ± 0.08 Tg C yr^{-1} for the Saribas (see Table 4). The contribution of CO to these terms is negligible.

4 Discussion

4.1 Sources and fate of carbon in the estuaries

4.1.1 Dissolved and particulate organic matter

It is striking that both DOC and CO_2 are higher in the estuaries than in the freshwater region. This means that carbon is not conservatively transported to the ocean and that a source of both DOC and CO_2 exists in the estuaries. C/N ratios in DOM (average: 40.6) clearly suggest a terrestrial origin (Fig. 4a). Based on the calculated zero-salinity end-members, we estimated that 15 % of the DOC in the Lupar and 3 % of the DOC in the Saribas estuary were derived from peat-draining tributaries. Given that peatlands cover 30.5 and 35.5 % of the catchments, we had expected a larger contribution. DOC concentrations in the Maludam river, the main river draining the Maludam peninsula, were more than ten times higher (3690 µmol L^{-1}, Müller et al., 2015) than the measured freshwater end-member of both Lupar and Saribas. If we assume that all peat-draining tributaries exhibit these high DOC concentrations, elevated DOC concentrations would have been expected in the estuaries as well. Even though the estuarine DOC maximum indicates that peat-draining tributaries are indeed relevant sources of DOC to the estuaries, their contribution is small measured against the extent of peatlands in the catchment. Thus, the simple assumption that high-DOC inputs are proportional to the peatland coverage is not valid in this case, probably because the peatlands are located very close to the coast (Müller et al., 2015).

Likely, a part of the DOC that reaches the Lupar and Saribas estuaries is also retained through adsorption and flocculation, which are promoted by mixing of saltwater and freshwater masses. Ertel et al. (1991) found that 1 to 12 % of DOC was converted to POC during laboratory experiments

Table 3. CO_2 and CO fluxes in the Lupar and Saribas estuaries determined with a floating chamber.

	FCO_2 (mol m^{-2} yr^{-1})			FCO (mmol m^{-1} yr^{-1})	
	LE	ME	UE	LE	ME
Lupar	14 ± 3	114 ± 27	60 ± 14	0.9 ± 0.2	1.8 ± 0.4
Saribas	n.d.	73 ± 61	33 ± 28	n.d.	0.7 ± 0.6
Saribas tributary	n.d.	268 ± 166	n.d.	n.d.	0.9 ± 0.6

LE: Lower estuariy (salinity > 25). ME: Mid-estuary (salinity 2–25, for the 2013 spatial extent of the rivers). UE: upper estuary.

Table 4. Total carbon fluxes estimated for the Lupar and Saribas aquatic systems. All numbers are in Tg C yr^{-1}.

	Lupar	Saribas	Total
Estuarine CO_2 emissions	0.30 ± 0.09	0.09 ± 0.08	0.39 ± 0.17
DOC export	0.12 ± 0.05	0.03 ± 0.01	0.15 ± 0.05
POC export	0.10 ± 0.12	0.03 ± 0.04	0.13 ± 0.16
TOC export	0.23 ± 0.17	0.06 ± 0.04	0.29 ± 0.21

due to changes in salinity. The transformation of DOC to POC in the presence of saltwater was attributed both to particle precipitation and to adsorption of DOM onto riverine particles. Due to the high SPM concentrations in the Lupar and Saribas estuaries, we think that these processes could be important as well. A partial conversion of DOC to POC is consistent with the high POC concentrations and with the C/N ratios in particulate organic matter (POM) (8.1–14.1). This is likely a mixed signal from marine and terrestrial sources (Fig. 4b), in agreement with the relatively low $\delta^{13}C$ values, which are indicative of both terrestrial soil and vascular plant material and phytoplankton (Bianchi and Bauer, 2011). We thus attribute those high POM concentrations to both river discharge and sediment resuspension due to the tidal currents.

In estuaries, POM may be degraded, deposited or exported to the continental shelf. It was shown that carbon burial in low-energy environments was a relevant sink of carbon in the Yangtze and Hudson estuaries (Zhu and Olsen, 2014). For example, 42 % of the carbon deposited on intertidal sediments of the Scheldt estuary was buried (Middelburg et al., 1995), suggesting that sediments can make a significant contribution to the retention of carbon in estuaries. On the other hand, sediments can also act as a source of DOC to the estuarine waters, as DOC is released during the respiration of POC in sediments. This represents another possible explanation for the enhanced DOC levels in the estuaries if compared to the measured freshwater end-member.

4.1.2 Controls on CO_2

The elevated pCO_2 in the Lupar and Saribas estuaries and the depletion of $\delta^{13}C$-DIC suggest that respiration plays an important role for the removal of organic matter (OM) in the estuaries as well. Respiration could take place in the water column (pelagic respiration) or in the sediments (benthic respiration).

Generally, pelagic respiration rates are largely controlled by temperature and the availability of organic substrates (Hopkinson Jr. and Smith, 2005). The relatively high concentrations of terrestrial organic matter (DOM + POM) and the high temperatures in the Lupar and Saribas estuaries suggest considerable rates of pelagic respiration, which would explain the relatively high pCO_2 and the correlation of CO_2 and AOU. The fact that this correlation was weak can be explained by the presence of other controls on CO_2 (pH, transport) as well as the buffering capacity of the carbonate system, whereas changes in CO_2 are buffered by DIC.

Estuarine pCO_2 is usually highest in high-turbidity zones (Abril and Borges, 2004), where the light penetration depth and thereby photosynthetic CO_2 uptake are limited. At the same time, the residence time of organic matter is prolonged (Abril et al., 1999), and particle-attached bacteria get the chance to decompose OM (Crump et al., 1998), resulting in pronounced net heterotrophy. Due to the strong tidal currents in the Lupar and Saribas estuaries, particle sedimentation is probably delayed by turbulence, leaving more time for the pelagic community to respire OM (Hopkinson Jr. and Smith, 2005).

Benthic respiration accounts on average for 24 % of the total system production in estuaries (Hopkinson Jr. and Smith, 2005). Although this respiration is largely aerobic, OM decomposition can also occur through denitrification, manganese, iron or sulfate reduction and methanogenesis. Middelburg et al. (1995) showed that 58 % of the carbon delivered to intertidal sediments in the Scheldt estuary was remineralized. The produced CO_2 may be detected in estuarine waters (Cai et al., 1999) or escape to the atmosphere from

the exposed sediment surface. This represents an additional CO_2 flux that we did not account for in our study. Therefore, future work should include the carbon supply to and remineralization rates in intertidal sediments.

Although pCO_2 is relatively high, oxygen depletion is quite moderate in comparison. For example, Chen et al. (2008) measured CO_2 partial pressures between 690 and 2680 µatm in the eutrophicated Pearl river estuary (see Table 5) along with AOU up to 239 µmol kg^{-1}, resulting in hypoxia at the river mouth. Although we found similarly high and even higher pCO_2, oxygen depletion was much less pronounced. This suggests that more oxygen is available in the Lupar and Saribas estuaries. Reaeration might be more efficient, i.e., oxygen fluxes across the air–water interface are higher, which could be explained by a high gas exchange velocity, consistent with our measurements, and a shallower water column.

Another important control on pCO_2 is pH, which varied spatially by 1.3 (2013) and 0.8 (2014) in the Lupar and Saribas estuaries. This can largely be attributed to the mixing of seawater and freshwater along the estuary, as indicated by the correlation of pH with salinity. Additionally, inputs from peat-draining rivers, which are highly acidic ($pH < 4$, Kselik and Liong, 2004; Müller et al., 2015), might decrease pH. Lower pH shifts the carbonate system towards more free CO_2, consistent with the elevated pCO_2 observed in the Lupar and Saribas estuaries. On the other hand, respiratory CO_2 might decrease pH. It cannot be ultimately resolved whether the pH drives pCO_2 or whether respiration drives the pH. In situ measurements of pelagic and benthic respiration rates could help resolve details about these mechanisms.

4.1.3 Photochemical degradation of organic matter

In addition to respiration, the diurnal CO cycle observed in the Lupar and Saribas estuaries (Fig. 7) suggests that photodegradation is another pathway for the removal of DOC. This diurnal pattern is well known for ocean surface water and explained by a balance of light-dependent production of CO and microbial consumption (Conrad and Seiler, 1980; Conrad et al., 1982; Ohta, 1997). Average CO concentrations in the Lupar and Saribas estuaries were lower than in the East China Sea and Yellow Sea (average 2.25 nmol L^{-1}, Yang et al. (2011); see Table 5), which can be attributed to the high turbidity. A high concentration of suspended particulates limits the light penetration depth and increases microbial CO consumption (Law et al., 2002). On the other hand, CO can also be photochemically produced from particles (Xie and Zafiriou, 2009). These authors found that in coastal waters, CO photoproduction from particulates was 10–35 % that of CDOM. We could not establish a clear relationship between SPM and CO for the Lupar and Saribas estuaries. However, the low CO concentrations suggest that particulates limited CO photoproduction rather than supported it. Another reason for the low CO concentrations could be that the terrestrial DOM in the Lupar and Saribas estuaries is not so susceptible to photodegradation, which would be in contrast to other studies (Valentine and Zepp, 1993; Zhang et al., 2006).

However, it would be too fast to conclude that photochemistry is only of little relevance for the DOM removal in our study area. First of all, most CO is probably produced directly at the water surface and might quickly escape to the atmosphere. We might not have captured this volatile CO fraction with our measurements, since we sampled water from 1 m below the surface. While CDOM absorption is highest in the UV (e.g., Kitidis et al., 2011), the attenuation of light in natural waters is strongest in the UV as well. Therefore, CO concentrations usually decline rapidly with water depth (Ohta et al., 2000), so the numbers presented here can be considered conservative. Secondly, the relevance of photochemistry amounts to more than CO production. UV radiation changes the composition of CDOM (Zhang et al., 2009), which changes its bioavailability (Amon and Benner, 1996; Moran et al., 2000). Tranvik et al. (2000) showed that in nutrient-poor (oligotrophic) systems, the net effect of radiation is an enhancement of bacterial growth, as photochemical reactions increased not only the bioavailability of organic carbon compounds, but also of nitrogen and phosphorous. However, other studies have shown that photochemical reactions consume molecular oxygen (Kitidis et al., 2014) and produce reactive oxygen species (ROS), which may decrease the bioavailability of DOM (Scully et al., 2003). Thus, the role of photochemistry in our study area beyond the mere production of CO remains uncertain and would merit further investigation.

4.2 Comparison dry season vs. wet season

Expectedly, the differences between dry season and wet season DOC were marginal, which is in agreement with other studies in this region. Moore et al. (2011) argued that DOC concentrations vary only little, because DOC is released to rivers throughout the year due to the high precipitation. They found that POC concentrations exhibited a clear seasonality, with higher concentrations during the dry season. Consistently, this was also observed in our study. The higher AOU and DIN values in the dry season indicate that respiration was higher then, possibly due to enhanced respiration of POC. The higher availability of POC in the dry season was most obvious in the Saribas and its tributary, whereas in the latter, the hypothesis of POC-enhanced respiration is confirmed by slightly higher pCO_2. For Lupar and the Saribas main river, though, we did not observe any major differences between wet and dry season pCO_2 and CO concentrations. The weak seasonal variability has some general implications for the research in our study area, which is mostly based on single campaigns and not on continuous measurements due to poor infrastructure. The little variation that we observe between our wet and dry season measurements could imply that sin-

Table 5. Comparison of CO_2 and CO values for partial pressure and concentration, respectively, and fluxes for different tropical and subtropical sites.

CO_2 site	pCO_2 (µatm)	FCO_2 (mol m^{-2} yr^{-1})	k model	Reference
Lower estuaries	640–662	14	FC	This study
in Sarawak, MY		2	W92	
Mid-estuaries	1849–5065	73–268	FC	This study
in Sarawak, MY		14–30	W92	
Upper estuaries	1021–1527	33–60	FC	This study
in Sarawak, MY		6–7	W92	
Malaysian estuaries	n.d.	0.4–6.3	W92	Chen et al. (2013)
Indonesian estuaries	n.d.	8.5–54.1	W92	Chen et al. (2013)
Pearl river estuary, CN	690–2680	n.d.	n.d.	Chen et al. (2008)
Brazilian estuaries	162–8638	0.3–63.9	RC01	Noriega and Araujo (2014)
Indian estuaries	300–18 492	−0.01–132.1	W92	Sarma et al. (2012)

CO site	CO (nmol L^{-1})	FCO (mmol m^{-2} yr^{-1})	k model	Reference
Lower estuaries	0.4–0.7	0.9	FC	This study
in Sarawak, MY		≤ 0.1	W92	
Mid-estuaries	0.4–1.3	0.7–1.8	FC	This study
in Sarawak, MY		0.1–0.2	W92	
Seto Inland Sea and Ise Bay, JP	n.d.	0.7–4.0	LM86	Ohta et al. (2000)
Equatorial Pacific	1.9–7.7	1.4–1.6	LM86	Ohta (1997)
Mauritanian upwelling	0.1–6.2	1.7–3.5	N00	Kitidis et al. (2011)
East China and Yellow Sea	0.1–7.0	0.4–6.8	W92	Yang et al. (2011)

The gas exchange velocity k used to calculate the flux was determined using different approaches: FC = floating chamber measurements. W92 = Wanninkhof (1992). N00 = Nightingale et al. (2000). LM86 = Liss and Merlivat (1986). RC01 = Raymond and Cole (2001).

gle measurement campaigns in this region provide better insights than previously assumed. However, measurements at the peak of the monsoon season would be desirable to confirm this hypothesis.

4.3 CO_2 and CO fluxes

It has been previously suggested that Southeast Asian estuaries are rather moderate sources of CO_2 to the atmosphere, because of low wind speeds and consequently low transfer velocities (Chen et al., 2013). We cannot confirm this notion with our measurements. CO_2 emissions from both the Lupar mid-estuary ($F_{CO_2,FC} = 114 \pm 27$ mol m^{-2} yr^{-1}) and the Saribas tributary ($F_{CO_2,FC} = 268 \pm 166$ mol m^{-2} yr^{-1}) are higher than the global average of 37.4 mol m^{-2} yr^{-1} for mid-estuaries (Chen et al., 2012). Certainly, elevated CO_2 fluxes can be partially attributed to high temperatures, which decrease the solubility of CO_2 in water and increase the gas exchange velocity. However, the average value reported for small deltas in this region is 41.8 mol m^{-2} yr^{-1} (Laruelle et al., 2013), which is also lower than the fluxes from Lupar and the Saribas tributary. The fluxes from the Saribas mid-estuary appear to be higher than those values, too ($F_{CO_2,FC} = 73 \pm 61$ mol m^{-2} yr^{-1}), but we cannot ascertain this because of the large uncertainty range. Interestingly, the fluxes that we found are also more than 1 order of magnitude higher than areal fluxes reported for Indian monsoonal estuaries (Sarma et al., 2012) and for other Malaysian rivers (Chen et al., 2013); see Table 5. However, flux estimates depend critically on the gas exchange velocity: both Sarma et al. (2012) and Chen et al. (2013) used the W92 parameterization for calculating the gas exchange velocity. The comparison between $F_{CO_2,FC}$ and $F_{CO_2,W92}$ revealed a considerable difference (see Table 5). However, $F_{CO_2,W92}$ in the mid-estuaries was still higher (14–30 mol m^{-2} yr^{-1}) than the values of Chen et al. (2013), and could indicate that the presence of peatlands makes a notable difference for CO_2 emissions from tropical estuaries.

CO flux estimates ($F_{CO,FC}$) were in a similar range as those obtained for the Mauritanian upwelling (Kitidis et al., 2011), and those reported for the equatorial Pacific upwelling (Ohta, 1997) and for the East China Sea and Yellow Sea (Yang et al., 2011) (see Table 5). However, if we use $F_{CO,W92}$ for comparison, it seems that CO fluxes are rather low in our study area, consistent with the observation that CO concentrations appear to be rather low, as discussed above.

Both the CO_2 flux estimates and the CO flux estimates presented in this study and elsewhere depend critically on the gas exchange velocity. The W92 exchange velocities differed considerably from our experimental values, yielding much lower fluxes. We believe that the W92 parameterization, which was derived for the ocean, is not suitable for estuaries, though frequently used. It does not account for the turbulence created by tidal currents and water flow velocity. Borges et al. (2004) showed that the contribution of the water-current related gas exchange velocity to the total gas exchange velocity was substantial at low wind speeds, which are prevalent in our case, too. Therefore, we think that it is more accurate to use empirically determined exchange velocities over wind speed parameterizations.

The performance of floating chambers has been a matter of debate. Arguments exist both for floating chambers leading to overestimation and underestimation of the flux: because they shield the water surface from wind, they may reduce the gas exchange (Frankignoulle, 1988). However, in our case, $k_{600,FC}$ were much higher than $k_{600,W92}$, so that here, the question is rather whether the floating chamber method leads to an overestimation of the flux. This would have been the case if the chamber had created artificial turbulences. Indeed, this has been discussed as one of the major weaknesses of the floating chamber method (Matthews et al., 2003; Vachon et al., 2010), although chambers are more susceptible to disruptions in low-turbulence environments than in high-turbulence environments (Vachon et al., 2010). In contrast, a recent study found a rather good agreement between floating chamber and eddy covariance measurements on a river (Huotari et al., 2013), which suggests that the accuracy of floating chamber measurements is also a matter of design. We intended to avoid creation of artificial turbulence by (1) using short wall extensions of the chamber into the water (ca. 1 cm), which is thought to decrease the artificial turbulence by making the chamber more stable (Matthews et al., 2003), and (2) letting the chamber float freely next to the boat. Our setup could be improved by monitoring the temperature in the chamber headspace, which was not done during this study. We assumed that the temperature increase was limited because of the short time of deployment (5–10 min).

Taken together, Lupar and Saribas deliver 0.3 Tg organic carbon to the South China Sea every year and release 0.4 TgC to the atmosphere as CO_2.

5 Conclusions

Overall, we conclude that these estuaries in a peat-dominated region receive considerable amounts of terrestrial organic carbon, only a minor part of which was contributed by peat-draining tributaries, however. Estuarine pCO_2 was largely driven by aerobic respiration of OM and pH variability. OM degradation was likely supported by photochemistry, as indicated by a diurnal variability of CO concentrations in the surface water. Overall, CO_2 emissions to the atmosphere were substantial if compared to other tropical and subtropical sites, while CO emissions were moderate, because photoproduction was limited by a high turbidity. We suggested that the use of a wind-driven turbulent diffusivity model (W92) leads to a gross underestimation of the fluxes, because it neglects turbulence caused by tidal currents and river discharge. Aside from net heterotrophy, we hypothesized that a fraction of the DOC was removed by adsorption onto estuarine particles. This highlights how these estuaries function as an efficient filter between land and ocean. Unlike small peat-draining rivers, which tend to export most organic carbon downstream, the adjacent estuaries seem to trap a large fraction of this terrestrial organic carbon. This means that the carbon export to the continental shelf is reduced, at the price of CO_2 production and, ultimately, emission from the estuary.

The Supplement related to this article is available online at doi:10.5194/bg-13-691-2016-supplement.

Acknowledgements. We would like to thank the Sarawak Biodiversity Center for permission to conduct research in Sarawak waters (permit no. SBC-RA-0097-MM and export permit SBC-EP-0040-MM). We thank Hella van Asperen (University of Bremen, Germany), Nastassia Denis, Felicity Kuek, Joanne Yeo, Hong Chang Lim, Edwin Sia (all Swinburne University, Malaysia) and all scientists and students from Swinburne University and the University of Malaysia Sarawak who were involved in the sampling campaigns and the preparation. Lukas Chin and the crew members of the SeaWonder are acknowledged for their extensive support. We would also like to acknowledge Innovasi Samudra Sdn Bhd for the loan of the CTD equipment. The authors thank Matthias Birkicht and Dorothee Dasbach (ZMT Bremen, Germany) for their help in the lab performing the analyses. Ultimately, we acknowledge the University of Bremen for funding this study through the "exploratory project" in the framework of the University's Institutional Strategy. The development of the FTIR measurements was supported by EU FP7 project InGOS. The authors thank three anonymous referees for their comments and suggestions which significantly improved the manuscript.

The article processing charges for this open-access publication were covered by the University of Bremen.

Edited by: M. Dai

References

Abril, G. and Borges, A. V.: Carbon Dioxide and Methane Emissions from Estuaries, in: Greenhouse Gas Emissions: Fluxes and Processes, Hydroelectric Reservoirs and Natural Environments, Environmental Science Series, Springer, Berlin, Heidelberg, New York, chapt. 7, 187–207, 2004.

Abril, G., Etcheber, H., Hir, P. L., Bassoullet, P., Boutier, B., and Frankignoulle, M.: Oxic/anoxic oscillations and organic carbon mineralization in an estuarine maximum turbidity zone (the Gironde, France), Limnol. Oceanogr., 44, 1304–1315, 1999.

Alkhatib, M., Jennerjahn, T. C., and Samiaji, J.: Biogeochemistry of the Dumai River Estuary, Sumatra, Indonesia, a tropical black-water river, Limnol. Oceanogr., 52, 2410–2417, 2007.

Amon, R. M. W. and Benner, R.: Photochemical and microbial consumption of dissolved organic carbon and dissolved oxygen in the Amazon River system, Geochim. Cosmochim. Ac., 60, 1783–1792, 1996.

Andriesse, J. P.: Nature and Manamanage of Tropical Peat Soils, FAO Soils Bulletin 59, Food and Agriculture Organization of the United Nations (FAO), Rome, 1988.

Baum, A.: Tropical blackwater biogeochemistry: the Siak River in central Sumatra, Indonesia, PhD thesis, University of Bremen, Bremen, Germany, 2008.

Baum, A., Rixen, T., and Samiaji, J.: Relevance of peat draining rivers in central Sumatra for the riverine input of dissolved organic carbon into the ocean, Estuar. Coast. Shelf S., 73, 563–570, 2007.

Bianchi, T. S. and Bauer, J. E.: Particulate Organic Carbon Cycling and Transformation, in: Treatise on Estuarine and Coastal Science, edited by: Wolanski, E. and McLusky, D. S., Vol. 5, 69–117, Academic Press, Waltham, 2011.

Borges, A. V., Vanderborght, J.-P., Schiettegatte, L.-S., Gazeau, F., Ferrón-Smith, S., Delille, B., and Frankignoulle, M.: Variability of the gas transfer velocity of CO_2 in a macrotidal estuary (the Scheldt), Estuaries, 27, 593–603, 2004.

Cai, W.-J., Pomeroy, L. R., Moran, M. A., and Wang, Y.: Oxygen and carbon dioxide mass balance for the estuarine-intertidal marsh complex of five rivers in the southeastern U.S., Limnol. Oceanogr., 44, 639–649, 1999.

Chen, C., Wang, S., Lu, X., Zhang, S., Lui, H., Tseng, H., Wang, B., and Huang, H.: Hydrogeochemistry and greenhouse gases of the Pearl River, its estuary and beyond, Quaternary Int., 186, 79–90, doi:10.1016/j.quaint.2007.08.024, 2008.

Chen C.-T. A., Huang, T.-H., Fu, Y.-H., Bai, Y., and He, X.: Strong sources of CO_2 in upper estuaries become sinks of CO_2 in large river plumes, Current Opinion in Environmental Sustainability, 4, 179–185, doi:10.1016/j.cosust.2012.02.003, 2012.

Chen, C.-T. A., Huang, T.-H., Chen, Y.-C., Bai, Y., He, X., and Kang, Y.: Air–sea exchanges of CO_2 in the world's coastal seas, Biogeosciences, 10, 6509–6544, doi:10.5194/bg-10-6509-2013, 2013.

Cole, J. J., Prairie, Y. T., Caraco, N. F., McDowell, W. H., Tranvik, L. J., Striegl, R. G., Duarte, C. M., Kortelainen, P., Downing, J. A., Middelburg, J. J., and Melack, J.: Plumbing the global carbon cycle: integrating inland waters into the terrestrial carbon budget, Ecosystems, 10, 171–184, doi:10.1007/s10021-006-9013-8, 2007.

Conrad, R. and Seiler, W.: Photooxidative production and microbial consumption of carbon monoxide in seawater, FEMS Microbiol. Lett., 9, 61–64, 1980.

Conrad, R., Seiler, W., Bunse, G., and Giehl, H.: Carbon monoxide in seawater (Atlantic Ocean), J. Geophys. Res., 87, 8839–8852, 1982.

Crump, B. C., Baross, J. A., and Simenstad, C. A.: Dominance of particle-attached bacteria in the Columbia River Estuary, USA, Aquat. Microb. Ecol., 14, 7–18, 1998.

Deutscher Wetterdienst (DWD): Climate Data Worldwide, available at: http://www.dwd.de/bvbw/appmanager/bvbw/dwdwwwDesktop?_nfpb=true&_pageLabel=_dwdwww_spezielle_nutzer_energiewirtschaft_historisch&T266071731411613450391O2gsbDocumentPath=NavigationFOeffentlichkeitFKlima__UmweltFKlimadatenFklimadaten__weltweitFdownload__node.htmlF__nnnDtrue (last access: 3 June 2015), 2007.

Dickson, A., Sabine, C., and Christian, G.: Guide to Best Practices for Ocean CO_2 Measurements, PICES Special Publications, 3rd Edn., North Pacific Marine Science Organization (PICES), 191 pp., 2007.

Duarte, C. M. and Prairie, Y. T.: Prevalence of heterotrophy and atmospheric CO_2 emissions from aquatic ecosystems, Ecosystems, 8, 862–870, doi:10.1007/s10021-005-0177-4, 2005.

Ertel, J. R., Alberts, J. J., and Price, M. T.: Transformation of riverine organic matter in estuaries, in: Proceedings of the 1991 Georgia Water Resources Conference, 19 and 20 March 1991, University of Georgia, Athens, Georgia, edited by: Hatcher, K. J., Institute of Natural Resources, The University of Georgia, 309–312, 1991.

FAO: Harmonized World Soil Database, FAO, Rome, Italy and IIASA, Laxenburg, Austria, 2009.

Frankignoulle, M.: Field measurements of air–sea CO_2 exchange, Limnol. Oceanogr., 33, 313–322, 1988.

Grasshoff, K., Kremling, K., and Ehrhardt, M.: Methods of Seawater Analysis, 3rd Edn., Verlag Chemie, Wiley-VCH, Weinheim, 1999.

Griffith, D. W. T.: Synthetic calibration and quantitative analysis of gas-phase FT-IR spectra, Appl. Spectrosc., 50, 59–70, 1996.

Griffith, D. W. T., Deutscher, N. M., Caldow, C., Kettlewell, G., Riggenbach, M., and Hammer, S.: A Fourier transform infrared trace gas and isotope analyser for atmospheric applications, Atmos. Meas. Tech., 5, 2481–2498, doi:10.5194/amt-5-2481-2012, 2012.

Hammer, S., Griffith, D. W. T., Konrad, G., Vardag, S., Caldow, C., and Levin, I.: Assessment of a multi-species in situ FTIR for precise atmospheric greenhouse gas observations, Atmos. Meas. Tech., 6, 1153–1170, doi:10.5194/amt-6-1153-2013, 2013.

Hopkinson Jr., C. S. and Smith, E. M.: Estuarine respiration: an overview of benthic, pelagic, and whole system respiration, in: Respiration in Aquatic Ecosystems, edited by: del Giorgio, P. A. and Williams, P. J. B., Oxford University Press, New York, 122–146, 2005.

Huotari, J., Haapanala, S., Pumpanen, J., Vesala, T., and Ojala, A.: Efficient gas exchange between a boreal river and the atmosphere, Gephys. Res. Lett., 40, 5683–5686, 2013.

Jähne, B., Münnich, K. O., Bösinger, R., Dutzi, A., Huber, W., and Libner, P.: On the parameters influencing air–water gas exchange, J. Geophys. Res., 92, 1937–1949, 1987.

Johnson, J. E.: Evaluation of a seawater equilibrator for shipboard analysis of dissolved oceanic trace gases, Anal. Chim. Acta, 395, 119–132, 1999.

Kitidis, V., Tilstone, G. H., Smyth, T. J., Torres, R., and Law, C. S.: Carbon monoxide emission from a Mauritanian upwelling filament, Mar. Chem., 127, 123–133, doi:10.1016/j.marchem.2011.08.004, 2011.

Kitidis, V., Tilstone, G. H., Serret, P., Smyth, T. J., Torres, R., and Robinson, C.: Oxygen photolysis in the Mauritanian upwelling: Implications for net community production, Limnol. Oceanogr., 59, 299–310, doi:10.4319/lo.2014.59.2.0299, 2014.

Kselik, R. A. L. and Liong, T. Y.: Hydrology of the Peat Swamp in Maludam National Park, Betong Division, Alterra Green World Research, Wageningen, The Netherlands/Forest Department Sarawak, Kuching, Malaysia/Sarawak Forestry Corporation, Kuching, Malaysia, 2004.

Kumagai, T., Saitoh, T. M., Sato, Y., Takahashi, H., Manfroi, O. J., Morooka, T., Kuraji, K., Suzuki, M., Yasunari, T., and Komatsu, H.: Annual water balance and seasonality of evapotranspiration in a Bornean tropical rainforest, Agr. Forest Meteorol., 128, 81–92, doi:10.1016/j.agrformet.2004.08.006, 2005.

Laruelle, G. G., Dürr, H. H., Lauerwald, R., Hartmann, J., Slomp, C. P., Goossens, N., and Regnier, P. A. G.: Global multi-scale segmentation of continental and coastal waters from the watersheds to the continental margins, Hydrol. Earth Syst. Sci., 17, 2029–2051, doi:10.5194/hess-17-2029-2013, 2013.

Law, C. S., Sjoberg, T. N., and Ling, R. D.: Atmospheric emission and cycling of carbon monoxide in the Scheldt Estuary, Biogeochemistry, 59, 69–94, 2002.

Lehner, B., Verdin, K., and Jarvis, A.: HydroSHEDS Technical Documentation, available at: http://hydrosheds.cr.usgs.gov (last access: 3 June 2015), World Wildlife Funds US, Washington, DC, 1.0 Edn., 2006.

Liss, P. S. and Merlivat, L.: Air–sea gas exchange rates: introduction and synthesis, in: The Role of Air–Sea Gas Exchange in Geochemical Cycling, edited by: Buat-Menard, P., NATO ASI Series, Reidel, Utrecht, 113–129, 1986.

Matthews, C. J. D., St. Louis, V. L., and Hesslein, R. H.: Comparison of three techniques used to measure diffusive gas exchange from sheltered aquatic surfaces, Environ. Sci. Technol., 37, 772–780, doi:10.1021/es0205838, 2003.

Middelburg, J. J., Klaver, G., Nieuwenhuize, J., and Vlug, T.: Carbon and nitrogen cycling in intertidal sediments near Doel, Scheldt Estuary, Hydrobiologica, 311, 57–69, 1995.

Miller, W. L. and Zepp, R. G.: Photochemical production of dissolved inorganic carbon from terrestrial organic matter: significance to the oceanic organic carbon cycle, Geophys. Res. Lett., 22, 417–420, 1995.

Moore, S., Gauci, V., Evans, C. D., and Page, S. E.: Fluvial organic carbon losses from a Bornean blackwater river, Biogeosciences, 8, 901–909, doi:10.5194/bg-8-901-2011, 2011.

Moore, S., Evans, C. D., Page, S. E., Garnett, M. H., Jones, T. G., Freeman, C., Hooijer, A., Wiltshire, A. J., Limin, S. H., and Gauci, V.: Deep instability of deforested tropical peatlands revealed by fluvial organic carbon fluxes, Nature, 493, 660–664, doi:10.1038/nature11818, 2013.

Moran, M. A., Sheldon Jr., W. M., and Zepp, R. G.: Carbon loss and optical property changes during long-term photochemical and biological degradation of estuarine dissolved organic matter, Limnol. Oceanogr., 45, 1254–1264, 2000.

Müller, D., Warneke, T., Rixen, T., Müller, M., Jamahari, S., Denis, N., Mujahid, A., and Notholt, J.: Lateral carbon fluxes and CO_2 outgassing from a tropical peat-draining river, Biogeosciences, 12, 5967–5979, doi:10.5194/bg-12-5967-2015, 2015.

Nightingale, P. D., Malin, G., Law, C. S., Watson, A. J., Liss, P. S., Liddicoat, M. I., Boutin, J., and Upstill-Goddard, R. C.: In situ evaluation of air–sea gas exchange parameterizations using novel conservative and volatile tracers, Global Biogeochem. Cy., 14, 373–387, 2000.

Noriega, C. and Araujo, M.: Carbon dioxide emissions from estuaries of northern and northeastern Brazil, Nature Scientific Reports, 4, 6164, doi:10.1038/srep06164, 2014.

Novelli, P. C. and Masarie, K. A.: Atmospheric Carbon Monoxide Dry Air Mole Fractions from the NOAA/ESRL Carbon Cycle Cooperative Global Air Sampling Network, 1988–2013, version: 2014-07-02, available at: ftp://aftp.cmdl.noaa.gov/data/trace_gases/co/flask/surface/ (last access: 3 June 2015), NOAA ESRL Global Monitoring Division, Boulder, Colorado, USA, 2014.

Ohta, K.: Diurnal variations of carbon monoxide concentration in the equatorial Pacific upwelling region, J. Oceanogr., 53, 173–178, 1997.

Ohta, K., Inomata, Y., Sano, A., and Sugimura, K.: Photochemical degradation of dissolved organic carbon to carbon monoxide in coastal seawater, in: Dynamics and Characterization of Marine Organic Matter, edited by: Handa, N., Tanoue, E., and Hama, T., TERRAPUB, Tokyo, 213–229, 2000.

Page, S. E., Rieley, J. O., and Banks, C. J.: Global and regional importance of the tropical peatland carbon pool, Glob. Change Biol., 17, 798–818, doi:10.1111/j.1365-2486.2010.02279.x, 2011.

Raymond, P. A. and Cole, J. J.: Gas exchange in rivers and estuaries: choosing a gas transfer velocity, Estuaries, 24, 312–317, 2001.

Raymond, P. A., Zappa, C. J., Butman, D., Bott, T. L., Potter, J. D., Mulholland, P., Laursen, A. E., McDowell, W. H., and Newbold, D.: Scaling the gas transfer velocity and hydraulic geometry in streams and small rivers, Limnol. Oceanogr.-Fluids & Environments, 2, 41–53, doi:10.1215/21573689-1597669, 2012.

Regnier, P., Friedlingstein, P., Ciais, P., Mackenzie, F. T., Gruber, N., Janssens, I. A., Laruelle, G. G., Lauerwald, R., Luyssaert, S., Andersson, A. J., Arndt, S., Arnosti, C., Borges, A. V., Dale, A. W., Gallego-Sala, A., Goddéris, Y., Goossens, N., Hartmann, J., Heinze, C., Ilyina, T., Joos, F., LaRowe, D. E., Leifeld, J., Meysman, F. J. R., Munhoven, G., Raymond, P. A., Spahni, R., Suntharalingam, P. and Thullner, M.: Anthropogenic perturbation of the carbon fluxes from land to ocean, Nat. Geosci., 6, 597–607, doi:10.1038/NGEO1830, 2013.

Sarma, V. V. S. S., Viswanadham, R., Rao, G. D., Prasad, V. R., Kumar, B. S. K., Naidu, S. A., Kumar, N. A., Rao, D. B., Sridevi, T., Krishna, M. S., Reddy, N. P. C., Sadhuram, Y., and Murty, T. V. R.: Carbon dioxide emissions from Indian monsoonal estuaries, Geophys. Res. Lett., 39, L03602, doi:10.1029/2011GL050709, 2012.

Scully, N. M., Cooper, W. J., and Tranvik, L. J.: Photochemical effects on microbial activity in natural waters: the interaction of reactive oxygen species and dissolved organic matter, FEMS Microbiol. Ecol., 46, 353–357, 2003.

Stubbins, A. P.: Aspects of Aquatic CO Photoproduction from CDOM, PhD thesis, University of Newcastle-upon-Tyne, Newcastle-upon-Tyne, 2001.

Tranvik, L. J., Olofsson, H., and Bertilsson, S.: Photochemical effects on bacterial degradation of dissolved organic matter in lake water, in: Microbial systems: new frontiers, edited by: Bell, C., Brylinsky, M., and Johnson-Green, P. Proceedings of the 8th International Symposium on Microbial Ecology, Halifax, 193–200, 2000.

Vachon, D., Prairie, Y. T., and Cole, J. J.: The relationship between near-surface turbulence and gas transfer velocity in freshwater systems and its implications for floating chamber measurements of gas exchange, Limnol. Oceanogr., 55, 1723–1732, doi:10.4319/lo.2010.55.4.1723, 2010.

Vähätalo, A. V.: Light, photolytic reactivity and chemical products, in: Biogeochemistry of Inland Waters, edited by: Likens, G. E., Elsevier/Academic Press, Amsterdam, 37–49, 2010.

Valentine, R. L. and Zepp, R. G.: Formation of carbon monoxide from the photodegradation of terrestrial dissolved organic carbon in natural waters, Environ. Sci. Technol., 27, 409–412, 1993.

Wanninkhof, R.: Relationship between wind speed and gas exchange over the ocean, J. Geophys. Res., 97, 7373–7382, 1992.

Weiss, R. F.: The solubility of nitrogen, oxygen and argon in water and seawater, Deep-Sea Res., 17, 721–735, 1970.

Weiss, R. F. and Price, B. A.: Nitrous oxide solubility in water and seawater, Mar. Chem., 8, 347–359, 1980.

Wiesenburg, D. A. and Guinasso Jr., N. L.: Equilibrium solubilities of methane, carbon monoxide, and hydrogen in water and seawater, J. Chem. Eng. Data, 24, 356–360, 1979.

Xie, H. and Zafiriou, O. C.: Evidence for significant photochemical production of carbon monoxide by particles in coastal and oligotrophic marine waters, Geophys. Res. Lett., 36, L23606, doi:10.1029/2009GL041158, 2009.

Yang, G.-P., Ren, C.-Y., Lu, X.-L., Liu, C.-Y., and Ding, H.-B.: Distribution, flux, and photoproduction of carbon monoxide in the East China Sea and Yellow Sea in spring, J. Geophys. Res., 116, C02001, doi:10.1029/2010JC006300, 2011.

Zafiriou, O. C., Xie, H., Nelson, N. B., Najjar, R. G., and Wang, W.: Diel carbon monoxide cycling in the upper Sargasso Sea near Bermuda at the onset of spring and in midsummer, Limnol. Oceanogr., 53, 835–850, 2008.

Zhang, Y., Xie, H., and Chen, G.: Factors affecting the efficiency of carbon monoxide photoproduction in the St. Lawrence estuarine system (Canada), Environ. Sci. Technol., 40, 7771–7777, doi:10.1021/es0615268, 2006.

Zhang, Y., Liu, M., Qin, B., and Feng, S.: Photochemical degradation of chromophoric dissolved organic matter exposed to simulated UV-B and natural solar radiation, Hydrobiologica, 627, 159–168, doi:10.1007/s10750-009-9722-z, 2009.

Zhu, J. and Olsen, C. R.: Sedimentation and Organic Carbon Burial in the Yangtze River and Hudson River Estuaries: Implications for the Global Carbon Budget, Aquat. Geochem., 20, 325–342, doi:10.1007/s10498-013-9191-x, 2014.